Simulation of Cookoff Results in a Small Scale Test

D.A. Jones and R.P. Parker

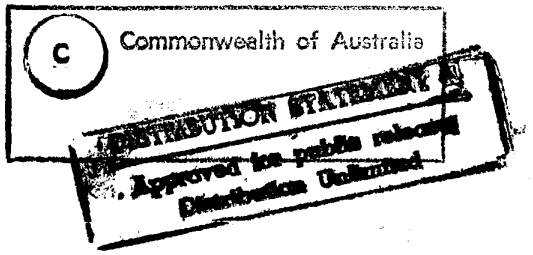

DEPARTMENT OF DEFENCE
DEFENCE SCIENCE AND TECHNOLOGY ORGANISATION

Simulation of Cookoff Results in a Small Scale Test

D.A. Jones and R.P. Parker

Explosives Ordnance Division
Aeronautical and Maritime Research Laboratory

DSTO-TR-0090

ABSTRACT

The fast and slow cookoff behaviour of two series of candidate insensitive booster compositions based on RDX/Elvax 210, and incorporating various amounts of PETN and TATB, has been numerically simulated using a one-dimensional finite difference code. The model solves a cylindrically symmetric heat flow equation for a mixture of two energetic materials with a time dependent boundary temperature. The temperature dependence of the thermal conductivity and specific heat of each of the explosives is included, as well as the effect of melting, and the effect of different kinetic schemes for the decomposition of the RDX. The simulations accurately reproduce the time to explosion and surface temperature at explosion for varying PETN concentration at both fast and slow heating rates, and also provide good agreement with experiment for varying TATB levels at the slow heating rate. However at the fast heating rate there is a divergence between the simulated results and experiment. The calculations clearly illustrate the need to include the temperature dependence of the thermal properties of the material, and a kinetic decomposition scheme appropriate to the degree of confinement, before good agreement between simulated and experimental results can be obtained.

Approved for public release

DEPARTMENT OF DEFENCE

DEFENCE SCIENCE AND TECHNOLOGY ORGANISATION

Published by

DSTO Aeronautical and Maritime Research Laboratory
GPO Box 4331
Melbourne Victoria 3001

Telephone: (03) 626 8111
Fax: (03) 626 8999

AR No. 008-959
October 1994

APPROVED FOR PUBLIC RELEASE

Simulation of Cookoff Results in a Small Scale Test

EXECUTIVE SUMMARY

The adoption of an Insensitive Munitions policy by the ADF has led to the requirement to develop an insensitive booster composition. A series of compositions based on the common military explosive RDX, coated with an ethylene-vinyl acetate copolymer Elvax 210, and containing varying amounts of the explosives PETN or TATB, has been tested experimentally for shock, impact and thermal sensitivity. None had sufficiently low thermal sensitivity to qualify as an insensitive booster composition.

To understand the thermal behaviour of these materials in more detail a mathematical model of the heat flow within the candidate booster compositions was developed and implemented in a one-dimensional computer code. The code was then used to simulate the experimental test procedures. It was found that the code could accurately predict the heat flow within the compositions in most cases, provided that allowance was made for the temperature dependence of the thermal properties of the explosives. It was also found that the rate of decomposition of the explosives depended strongly on the degree of confinement, and that a kinetic decomposition scheme appropriate to the strength of the confinement was needed before good agreement with experiment was obtained. The material models developed in this study can now be used in more advanced computer codes which attempt to predict the degree of violence of the thermal response.

Authors

D.A. Jones
Explosives Ordnance Division

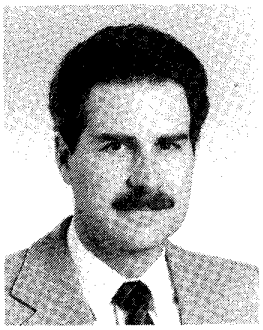

David Jones graduated from Monash University in 1972 with a BSc (Hons). He obtained his PhD from Monash in 1976. His thesis was titled "Anisotropic diffusion in the Townsend-Huxley experiment". After working at Strathclyde University, London University and the University of New South Wales he joined AMRL in 1983. He has worked on the numerical modelling of shaped charge warheads and slapper detonator devices. From February 1987 to May 1988 he was a Visiting Scientist at the Laboratory for Computational Physics and Fluid Dynamics at the Naval Research Laboratories in Washington DC. While there he worked on advanced computational fluid dynamics.

R.P. Parker
Explosives Ordnance Division

Robert Parker graduated Dip App Chem from Ballarat School of Mines and Industries in 1968, and joined AMRL in that year. He has worked exclusively on explosive materials; his present major areas of interest are cookoff of explosives and PBX formulations.

Contents

1. Introduction

A recent MRL Report described the preparation and characterisation of three series of candidate insensitive booster compositions based on RDX/Elvax 210 and incorporating various amounts of PETN, DATB or TATB [1]. Each composition was characterised for impact sensitiveness, shock sensitivity and cookoff behaviour. One of the compositions had suitable shock and impact sensitiveness, but none of them exhibited sufficient reduction in cookoff reaction violence to give an acceptable insensitive booster composition.

In an effort to gain a greater understanding of the behaviour of energetic materials when subjected to heating at various rates, we have numerically simulated the thermal environment in the Super Small-scale Bomb Test (SSCB) for two of the candidate insensitive booster compositions described by Dagley et al. [1]. Our model solves the one-dimensional cylindrically symmetric heat flow equation for a mixture of two energetic materials with a time dependent boundary temperature. Our work is similar in many respects to recent papers by Drake [2], and McGuire and Tarver [3], which model time to explosion in One Dimensional Time to Explosion experiments (ODTX), but there are important differences. The ODTX experiments impose a constant boundary temperature at the surface of a heavily confined, spherical explosive sample, whereas the SSCB test applies a steadily increasing temperature to the surface of a more lightly confined explosive, and tests are typically conducted at both fast (approximately 1°C/second) and slow (approximately 0.1°C/second) heating rates.

We implemented the model in two stages. In the first stage we used a zero order kinetic scheme with an Arrhenius temperature dependent rate coefficient to describe the decomposition of the explosives, and we assumed that the specific heat and thermal conductivity of the compositions were independent of temperature. This simple model was sufficient to explain the trends in the data observed by Dagley et al., but in general the simulated results were lower than the experimental values for both time to ignition and the surface temperature at ignition.

We then considered several refinements to the model, including a three term kinetic scheme for the decomposition of the RDX, and allowance for the temperature dependence of the thermal conductivity and specific heat of the materials. Where appropriate, these were included in the calculations, and generally lead to improved agreement of the simulated results with experiment.

No attempt has been made at this stage to model the violence of the reaction event. Current understanding of the physical processes involved in the transition to either deflagration or detonation in a cookoff event is vague [4], although encouraging progress on the problem has been made recently by Cook and Haskins [5].

2. Simplified Model

Dagley et al. [1] chose RDX/Elvax 210 (95:5) as the reference composition and from this mixtures containing TATB and PETN at levels ranging from 5% to 35% were prepared (all samples were pressed to 90% TMD), and their cookoff response was determined in the Super Small-scale Cookoff Bomb. The SSCB has been described in detail by Parker [6], and a recent report by Jones and Parker [7] described numerical simulations of heat flow in the related Small-scale Cookoff Bomb. One of the conclusions of that report was that the temperature distribution within the SCB could be accurately described using a one-dimensional heat flow model, and so we have adopted a similar one-dimensional model for the SSCB.

2.1 Numerical Solution

The radial heat flow in the SSCB for a multi-component explosive mixture is described by the following equation [8]:

$$\rho C \frac{\partial T}{\partial t} - \lambda \left\{ \frac{\partial^2 T}{\partial r^2} + \frac{1}{r} \frac{\partial T}{\partial r} \right\} = S \qquad (1)$$

where ρ is density, C is specific heat, λ is the thermal conductivity of the mixture, T is temperature, t is time, and r is radial distance. S describes the rate of heat generation per unit volume at temperature T. If we neglect reactant depletion (ie. zero order kinetics) and assume that the rate of reaction of each of the species varies in accordance with the Arrhenius equation then S has the form

$$S = \sum_{s=1}^{NS} \rho \overline{m}_s Q_s A_s \exp\left[-E_s / RT\right] \qquad (2)$$

where $\overline{m}_s$ is the mass, Q_s the heat of reaction per unit mass, A_s the pre-exponential factor, E_s the activation energy, and NS is the total number of species. R is the gas constant.

Equation (1) is solved using an operator splitting technique. First the source term is set to zero and the equation is discretised using a standard Forward Time Centred Space (FTCS) scheme [9]. This results in the following explicit equation for the temperature at the (n+1)th time step at node i in terms of the temperatures at the nth time step at nodes *i*-1, *i*, and *i*+1

$$T_i^{n+1} = T_i^n + \frac{\alpha \Delta t}{\Delta r^2} \left\{ \left[1 + \frac{1}{2(i-1)} \right] T_{i+1}^n - 2T_i^n + \left[1 - \frac{1}{2(i-1)} \right] T_i^n{}_1 \right\} \qquad (3)$$

where α is the thermal diffusivity and is defined by

$$\alpha = \frac{\lambda}{\rho C} \tag{4}$$

Equation (3) does not apply on the axis of the cylinder where i=1. For this special case we apply L'Hopital's rule to the third term on the left side of equation (1) to show that

$$\frac{1}{r}\frac{\partial T}{\partial r} \rightarrow \frac{\partial^2 T}{\partial r^2} \text{ as } r \rightarrow 0$$

Equation (1) then becomes

$$\rho C \frac{\partial T}{\partial t} - 2\lambda \frac{\partial^2 T}{\partial r^2} = S \tag{5}$$

and has a finite difference representation of the form

$$T_i^{n+1} = T_i^n + \frac{2\alpha \Delta t}{\Delta r^2}\left\{2T_{i+1}^n - 2T_i^n\right\} \tag{6}$$

where continuity of the derivative on the axis has also been used in deriving the finite difference form. Solutions to equations (3) and (6) are stable provided that the time step Δt and spatial step Δr satisfy the following inequality

$$\frac{\alpha(\Delta t)}{(\Delta r)^2} < \frac{1}{2} \tag{7}$$

In the simulation results presented here Δt was always chosen to be considerably less than the minimum value imposed by equation (7), and several values of Δt and Δr were used to ensure that the results were independent of the spatial and time step resolution.

Solution of equation (1) proceeds by updating the temperature at each node point at the end of a time step Δt using either equation (3) (for $i \neq 1$) or equation (6) (for i=1). The special case i=N corresponds to the surface of the SSCB. The temperature at this point is obtained from a look-up table which lists the experimentally measured temperature as a function of time at the surface of the SSCB for both fast and slow cookoff. These values were determined during calibration runs using an SSCB with an inert material whose thermal properties closely matched those of the explosive fills. The temperature increase due to the decomposition of the explosive is then included by updating the temperature at each node point from the source term S using the expression

$$T_i^{n+1} = T_i^{n+1} + \Delta t \sum_{s=1}^{NS} \overline{m}_s Q_s A_s \exp\left[-E_s / R T_i^{n+1}\right] \tag{8}$$

RDX melts at a temperature of 204°C, and as the surface temperature at ignition under fast cookoff conditions for RDX/Elvax 210 (95:5) is 240°C an appreciable fraction of the RDX content in the SSCB will be present in the liquid state. Similar comments apply for slow cookoff, where the surface temperature at reaction is 218°C. Hence it is important to include the effect of melting. We did this using the following procedure; as soon as the temperature at a particular node reached the melting point of the material we held the temperature at that node constant at the melting point value until an energy equivalent to the latent heat of fusion of the material had been absorbed. In the simple model presented in this section we allowed only the RDX component to undergo melting. PETN however has a lower melting point of 140°C, and we have allowed for melting of both components in a two component mixture in a later section.

2.2 Material Parameters

Solution of equation (1) for a two component explosive mixture requires specification of the thermal conductivity, specific heat, density, heat of reaction, pre-exponential factor and activation energy for each of the component species. In the simplified model used here we have made the approximation that the value of each of these material properties is independent of temperature. Choosing appropriate values for each of these parameters is difficult however as there are considerable discrepancies between some of the values quoted in the literature.

The thermal conductivity (at room temperature) of RDX is given by Rogers [10] as 2.53×10^{-4} cal cm^{-1} s^{-1} $°C^{-1}$, by Zinn and Mader [11] as 7×10^{-4} cal cm^{-1} s^{-1} $°C^{-1}$, and by McGuire and Tarver [3] and Drake [2] as 6.22×10^{-4} cal cm^{-1} s^{-1} $°C^{-1}$. There is less disagreement regarding the value of the specific heat of RDX at room temperature; Dobratz and Crawford [12] quote a value of 0.26×10^{-4} cal g^{-1} $°C^{-1}$, while McGuire and Tarver use 0.24×10^{-4} cal g^{-1} $°C^{-1}$. There are also discrepancies in the values for the activation energy, pre-exponential factor, and heat of reaction for RDX. Zinn and Mader use E = 47.5 kcal M^{-1}, A = 3.162×10^{18} s^{-1} and Q = 500 cal g^{-1}, Rogers uses E = 47.1 kcal M^{-1} , A = 2.02×10^{18} s^{-1} and Q = 500 cal g^{-1}, while Hutchinson [13] uses E = 48.5 kcal M^{-1}, A = 8.6×10^{18} s^{-1} and Q = 549 cal g^{-1}.

The values we have chosen for RDX are shown in Table 1. These were determined by performing a number of numerical simulations of the time to reaction and temperature at reaction for RDX for both fast and slow cookoff events, and then chosing those values which gave the best overall fit to the experimental results. The values chosen for specific heat and thermal conductivity also have the advantage of agreeing with the temperature dependent values of these quantities at room temperature, which will facilitate comparisons with experiment in a later section where we specifically include the effect of the temperature dependence of these properties.

Table 1: Thermochemical Constants

	RDX	PETN	TATB
Density (g.ml $^{-1}$)	1.80	1.74	1.84
Thermal conductivity (cal cm^{-1}s^{-1} °C^{-1})	0.00062	0.0006	0.00191
Specific Heat (cal g^{-1}°C^{-1})	0.24	0.272	0.26
A (s^{-1})	3.162×10^{18}	6.300×10^{19}	3.180×10^{19}
Q (cal g^{-1})	500	300	600
E (kcal M^{-1})	48.0	47.0	59.9
Latent Heat of Fusion (cal g^{-1})	38.4	10.0	-
Melting Point (°C)	204	141	320

The values used for PETN and TATB have been taken primarily from the paper by Rogers [10], although the specific heat and thermal conductivity values have been taken from the more recent papers by McGuire and Tarver [3], and Drake [2]. Calculations were also performed at both crystal density and 90% TMD, and it was found that the slight change in density had a negligible effect on the results.

Table 2 shows the calculated time to explosion and surface temperature at reaction for RDX/Elvax 210 (95:5) for both fast and slow cookoff conditions using the values for the physical constants shown in Table 1 (the values in brackets are the percentage deviation from the experimental results). The effect of the Elvax 210 on the behaviour of RDX has been neglected at this stage, and we will discuss this point in more detail in a later section. Thermal explosion was considered to have occured when the temperature at some point in the explosive reached a predetermined high value. For the calculations reported here this value was 550 °C, although the actual value used had negligible effect on the results. The calculations were performed both with and without the inclusion of melting, and the results clearly show the importance of including this effect, particularly for the slow cookoff results.

Table 2: Simulated results for RDX/Elvax 210 (95:5)

FAST COOKOFF			
	Melting Neglected	Melting Included	Experiment
Time to Event (s) Surface Temp. °C	242 (1.6%) 232 (3.3%)	256 (3.6%) 241 (0.4%)	246 240
SLOW COOKOFF			
	Melting Neglected	Melting Included	Experiment
Time to Event (s) Surface Temp. °C	1208 (27%) 195 (11%)	1461 (11.7%) 210 (3.6%)	1654 218

The results shown in Table 2 will be improved in a later section when we consider a more accurate model for RDX, but they are adequate as a starting point for modelling the effect of the addition of varying amounts of PETN and TATB on the cookoff behaviour of RDX/Elvax 210.

To calculate the thermal conductivity of the explosive mixtures we have used an expression originally derived by Maxwell [14], and more recently by Jeffrey [15], who derived an expression for the thermal conductivity to a higher order in the species concentration. Jeffrey studied the conduction of heat through a stationary, random and statistically homogeneous suspension of spherical particles in a matrix of uniform conductivity under the condition that the volume fraction of the particles is small. If the matrix has thermal conductivity λ_1, and the spheres a thermal conductivity λ_2, then to first order in the concentration c the effective conductivity λ is given by

$$\lambda = \lambda_1\{1 + 3\beta c\} \tag{9}$$

where

$$\beta = (\lambda_2 - \lambda_1)/(\lambda_2 + \lambda_1) \tag{10}$$

Equation (9) is valid when the concentration is small enough to make all interactions between the spheres negligible. Jeffrey has extended the expression for λ to second order in c by allowing for interactions between pairs of spheres, but in keeping with the simplicity of the model adopted for each of the explosive components we have calculated the thermal conductivity of the mixture using the lower order correction only. Use of equation (9) gives results which are very close to those calculated by assuming that the thermal conductivity of the mixture is simply given by the mass average of the values for the individual explosives, which is the method used by McGuire and Tarver in their calculations [3].

3. Results of Simplified Model

As described by Dagley et al [1], TATB and PETN were added to the RDX/Elvax 210 (95:5) reference composition to modify its cookoff response by incorporating explosives having different thermal stabilities. TATB has a much higher critical temperature than RDX and was expected to act as an inert material during the heating phase, thus lowering the explosive output during accidental thermal stimulus, but retaining full explosive output when initiated in the normal manner. PETN has a lower critical temperature and was expected to lead to reaction at lower temperatures and to produce milder responses due to early release of confinement resulting from the initial reaction of the PETN.

At the slow heating rate both the PETN and the TATB succeeded in moderating the violence of the cookoff reaction. As the PETN content increased the explosive surface

temperature at reaction decreased and milder responses were also obtained in most cases. Figure 1 shows the experimental results and the predictions of the model for the surface temperature at reaction as a function of PETN content for the slow heating rate. (In all the Figures presented here the open circles represent the experimental results and the filled circles represent the simulated results. The dashed line through the experimental data typically denotes a second order polynomial fit to the data, and the solid line a second order polynomial fit to the model results.) As noted in the previous section, the simple model employed here uses temperature independent values for the specific heat and thermal conductivity for each explosive, and the particular values chosen give a better fit to the data for RDX/Elvax 210 (95:5) at the fast heating rate rather than at the slow heating rate. This is the cause of the offset between the two curves in Figure 1. Apart from this discrepancy, the model provides a good qualitative explanation of the trend in the experimental data. As expected, the decrease in surface temperature at reaction is due to the PETN content undergoing thermal runaway before the RDX begins to react appreciably. If the RDX source term is omitted from equation (2) then almost identical results are obtained, indicating that the thermal runaway is triggered by the PETN. Figure 2 shows the time to reaction as a function of PETN content for the slow heating rate and similar results are obtained. Again the decrease in time to reaction as the percentage of PETN in the composition is increased is qualitatively reproduced by the model.

For different levels of TATB at the slow heating rate the reactions generally occurred in the same temperature range as the RDX/Elvax 210, indicating that the reaction was being triggered by the RDX, and the cookoff responses were generally milder than for the reference composition. Figure 3 shows the experimental results and the predictions of the model for the surface temperature at reaction as a function of TATB content for the slow heating rate. The experimental results show a very slight increase in surface temperature at reaction as the TATB content is increased and the model accurately reproduces this trend, with the rate of increase in temperature being very similar for both curves. Again there is an approximately constant offset between the two lines because of the nature of the model used for the RDX/Elvax 210 (95:5) composition. The very small effect which the TATB has on the surface temperature at reaction is due to the very slight change in thermal conductivity of the mixture. The TATB is thermally very stable in the temperature range shown in Figure 3 and the reaction is triggered by the RDX. Removal of the TATB source term in equation (2) leads to exactly the same results.

Figure 4 shows the time to reaction as a function of TATB content for the slow heating rate. The model predicts a steady increase in time to reaction as the TATB content increases whereas a straight line fit to the experimental data indicates a decrease in time to reaction as TATB content increases. There is considerable scatter in the experimental data shown in Figure 4 however and more data is required to get a true representation of the experimental trend.

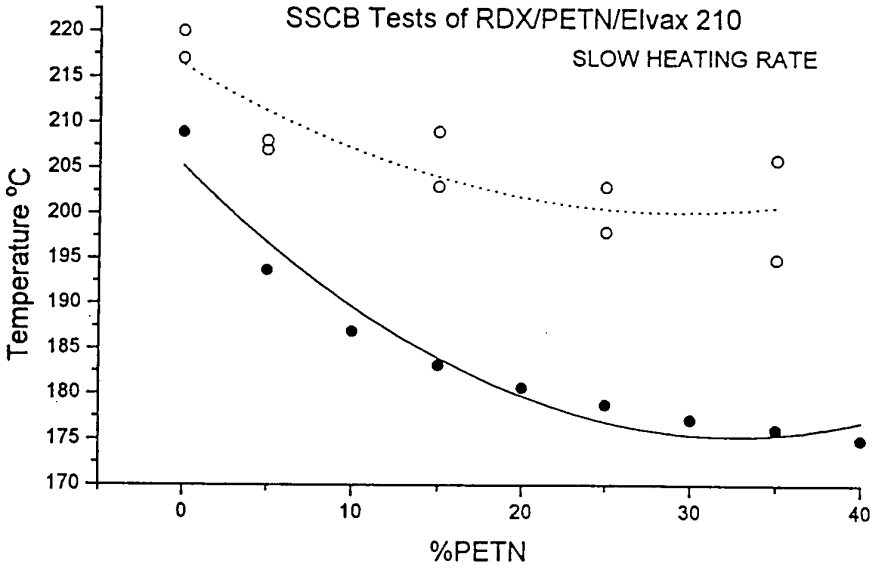

Figure 1: Surface temperature at reaction as a function of PETN content. The open circles are the experimental points and the filled circles are the predictions of the simple model.

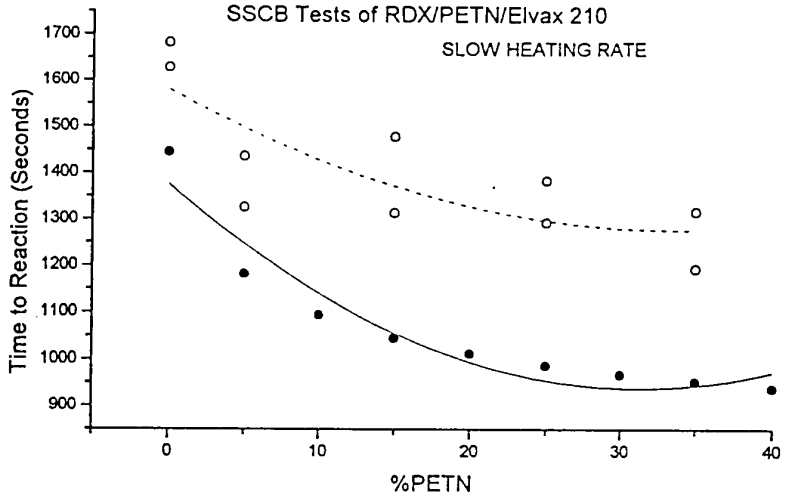

Figure 2: Time to reaction as a function of PETN content. The open circles are the experimental points and the filled circles are the predictions of the simple model.

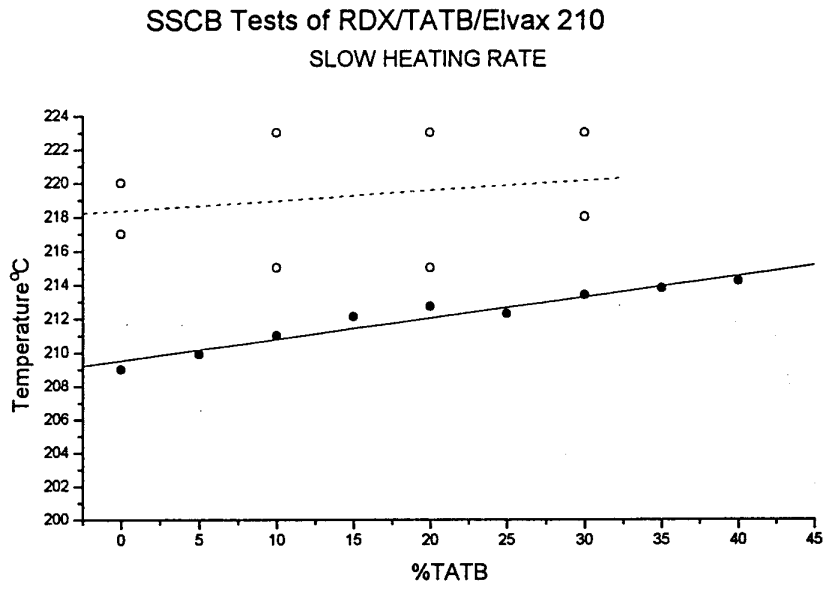

Figure 3: Surface temperature at reaction as a function of TATB content. The open circles are the experimental points and the filled circles are the predictions of the simple model.

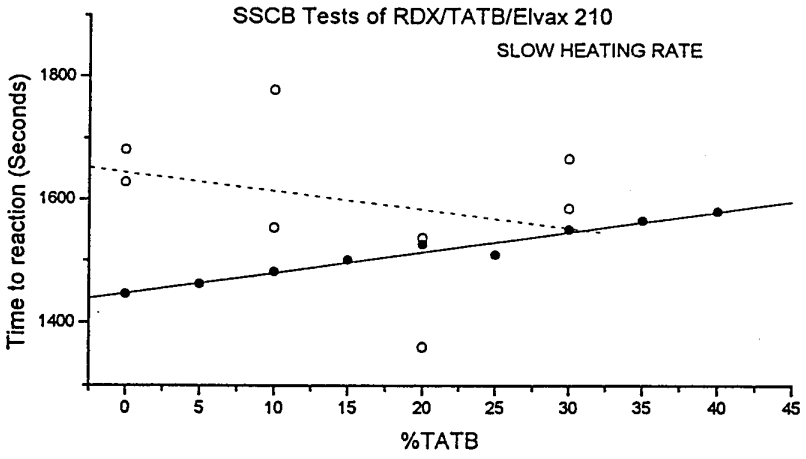

Figure 4: Time to reaction as a function of TATB content. The open circles are the experimental points and the filled circles are the predictions of the simple model.

At the fast heating rate addition of PETN had no appreciable effect on the reaction temperature until a considerable amount of PETN (25%-35%) had been added, and all the compositions gave more violent responses than the reference composition. Figure 5 shows the experimental results and the predictions of the model for the surface temperature at reaction as a function of PETN content for the fast heating rate. The experimental results are again quite scattered, but the overall trend is to a slow decrease in surface temperature at reaction for small percentages of PETN, followed by a more rapid decrease at higher concentrations. The model however predicts the reverse, with the maximum decrease in surface temperature occurring at low concentrations of PETN and then the temperature appears almost to level off for higher concentrations. Similar results are shown in Figure 6, where we plot the time to reaction as a function of PETN content at the fast heating rate. At low PETN concentrations the two curves show opposing trends, with the experimental values increasing with concentration and the model predictions decreasing with concentration. These conflicting results may be due to some of the assumptions made in the simple model, particularly the assumption of temperature independent values for the thermal conductivity and specific heat. We will pursue this point further in the next section.

The addition of TATB had little effect on either reaction temperature or response at the fast heating rate; reaction continued to occur in the same temperature range as for the RDX/Elvax 210, and the responses were generally similar to those of the RDX/Elvax 210. Figure 7 shows the experimental results and the predictions of the model for the surface temperature at reaction as a function of TATB content for the fast heating rate. The experimental results are fairly scattered but show a trend towards a very slight increase in surface temperature at reaction as the TATB content is increased. The model similarly predicts an increase in temperature with increasing TATB content.

Figure 8 shows the time to reaction as a function of TATB content for the fast heating rate. The experimental data is extremely scattered, but shows a trend towards increasing temperatures with increasing TATB content. This is also predicted by the model, although the rate of increase is much slower than that shown experimentally. The discrepancy between the results is probably a combination of insufficient experimental data and the inadequacy of some of the assumptions employed in the model.

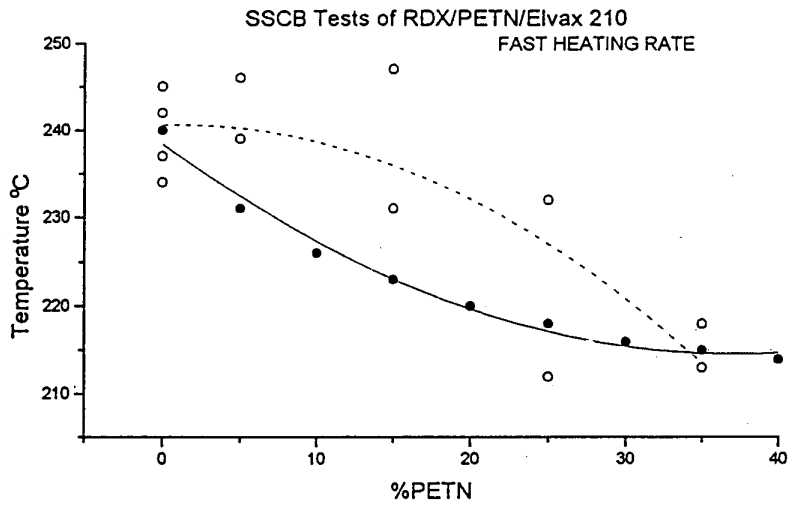

Figure 5: Surface temperature at reaction as a function of PETN content. The open circles are the experimental points and the filled circles are the predictions of the simple model.

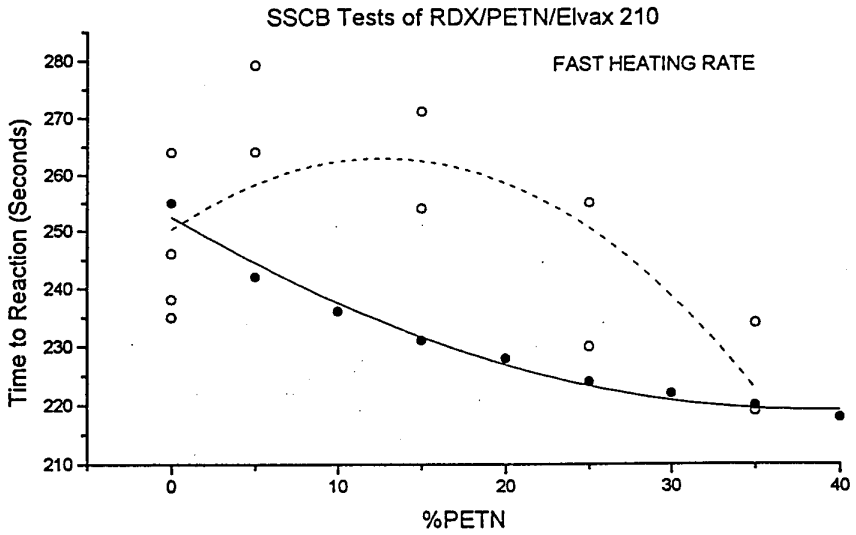

Figure 6: Time to reaction as a function of PETN content. The open circles are the experimental points and the filled circles are the predictions of the simple model.

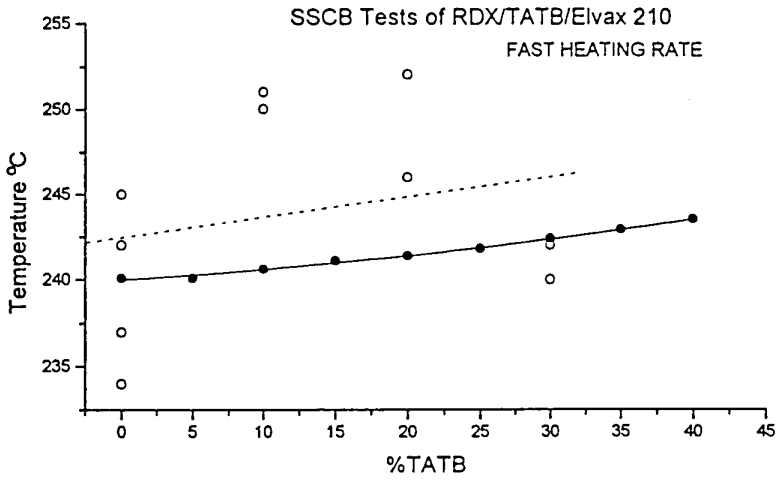

Figure 7: Surface temperature at reaction as a function of TATB content. The open circles are the experimental points and the filled circles are the predictions of the simple model.

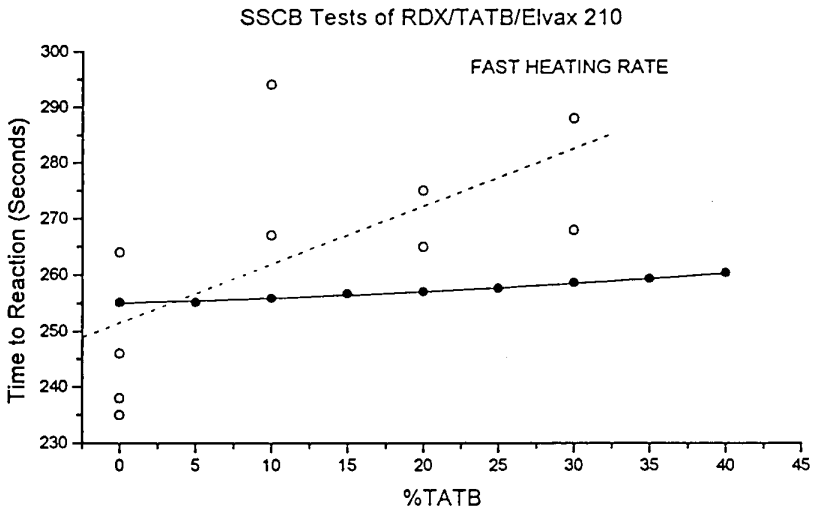

Figure 8: Time to reaction as a function of TATB content. The open circles are the experimental points and the filled circles are the predictions of the simple model.

4. Improved Model

Since the early work of Rogers [10], Zinn and Mader [11], and Zinn and Rogers [16], more refined models of the thermal behaviour of many explosives have appeared in the literature. Prominent among these is the work of Catelano et al. [17], Tarver et al. [18], and McGuire and Tarver [3]. These authors have considered thermal decomposition of confined explosives in one-dimensional geometries and have obtained good agreement between experimental results and calculations in One-Dimensional-Time-to-Explosion (ODTX) tests. The calculated results include the temperature dependence of the specific heat and thermal conductivity, as well as multi-term schemes for the decomposition reactions. In this section we implement the model for RDX described by McGuire and Tarver [3] and consider the effect of these improvements on the calculated time to explosion and surface temperature for the SSCB test on RDX/Elvax 210.

4.1 Temperature Dependant Thermal Properties

When the thermal conductivity and specific heat are temperature dependant, the radial heat flow in the SSCB is described by the following equation [19]

$$\rho C(T)\frac{\partial T}{\partial t} = \frac{\partial}{\partial r}\left(\lambda(T)\frac{\partial T}{\partial r}\right) + \frac{2\lambda(T)}{r}\frac{\partial T}{\partial r} + S \qquad (11)$$

The finite difference form of equation (11) is found by replacing each of the differential terms by the following expressions [20]

$$\rho C(T)\frac{\partial T}{\partial t} \rightarrow \rho_i^n C_i^n (T_i^{n+1} - T_i^n)/\Delta t \qquad (12)$$

$$\frac{\partial}{\partial r}\left(\lambda(T)\frac{\partial T}{\partial r}\right)_i^n \rightarrow \lambda_{i+1/2}^n\left(\frac{T_{i+1}^n - T_i^n}{\Delta r^2}\right) - \lambda_{i-1/2}^n\left(\frac{T_i^n - T_{i-1}^n}{\Delta r^2}\right) \qquad (13)$$

$$\left(\frac{2\lambda(T)}{r}\frac{\partial T}{\partial r}\right)_i^n \rightarrow \frac{2\lambda_i^n}{(i-1)\Delta r}\left[\frac{T_{i+1}^n - T_{i-1}^n}{2\Delta r}\right] \text{... for i}\neq 1 \qquad (14)$$

$$\left(\frac{2\lambda(T)}{r}\frac{\partial T}{\partial r}\right)_i^n \rightarrow \frac{2\lambda_i^n}{\Delta r^2}\left[2T_{i+1}^n - 2T_i^n\right] \text{..... for i=1} \qquad (15)$$

where $\lambda_{i+1/2}^n$ and $\lambda_{i-1/2}^n$ are defined by

$$\lambda^n_{i+1/2} = \frac{1}{2}\left(\lambda^n_{i+1} + \lambda^n_i\right) .. \text{ and } .. \lambda^n_{i-1/2} = \frac{1}{2}\left(\lambda^n_i + \lambda^n_{i-1}\right), \qquad (16)$$

which results in the following expression for the temperature at the (n+1)th time step at node i

$$T^{n+1}_i = T^n_i + \frac{\Delta t}{(\Delta r)^2}\frac{\lambda^n_i}{\rho C^n_i}\left\{T^n_{i+1}\left(\frac{\lambda^n_{i+1/2}}{\lambda^n_i} + \frac{1}{2[i-1]}\right) - T^n_i\left(\frac{\lambda^n_{i+1/2}}{\lambda^n_i} + \frac{\lambda^n_{i-1/2}}{\lambda^n_i}\right) + T^n_{i-1}\left(\frac{\lambda^n_{i-1/2}}{\lambda^n_i} - \frac{1}{2[i-1]}\right)\right\}$$

for i≠1, and

$$T^{n+1}_i = T^n_i + \frac{4\lambda^n_i}{\rho C^n_i}\frac{\Delta t}{(\Delta r)^2}\left\{T^n_{i+1} - T^n_i\right\} \text{.....for i=1} \qquad (18)$$

Solution of equation (11) proceeds in an iterative fashion. We begin with an initial value for the temperature at all grid points. Values for the thermal conductivity and specific heat are then calculated and equations (17) and (18) solved to get the new temperature values. New values for the thermal conductivity and specific heat are then calculated using the new temperature values and then equations (17) and (18) are solved again to get new estimates for the temperature. The cycle is repeated until successive changes in temperature fall below some prescribed small limit. The temperature increase from the source term is then added in the same manner as before, and the cycle is then repeated for the next time step.

We have also included the effect of reactant depletion at this stage by writing the source term as

$$S = \rho Q A \omega \exp\left[-E/RT\right] \qquad (19)$$

where ω is the mass fraction of undecomposed RDX. The time dependence of ω is described by

$$\frac{\partial \omega}{\partial t} = -A\omega \exp\left[-E/RT\right] \qquad (20)$$

As an illustration of the effect of the inclusion of temperature dependent thermal properties and reactant depletion, the time to explosion and surface temperature have been calculated for RDX in the SSCB for both fast and slow cookoff. The temperature dependence of the specific heat and thermal conductivity were taken from the paper by McGuire and Tarver [3]. Over the temperature range considered the thermal conductivity of the RDX decreases by approximately 30% to 40% as the temperature increases, while the specific heat increases by approximately 50%. The results are presented in Table 3 (the experimental values are for the reference composition, RDX/Elvax 210 (95:5), not pure RDX). These figures show that the inclusion of both these effects has a marked effect on the calculated times and temperatures for the

SSCB cookoff tests. Agreement with experiment has been improved considerably for slow cookoff, and even the fast cookoff results have improved slightly.

Table 3: Simulated results for RDX/Elvax 210 (95:5) using Improved Model

FAST COOKOFF			
	λ and C fixed	λ and C variable	Experiment
Time to Event (s) Surface Temp. °C	258 (5%) 242 (1%)	256 (4%) 241 (1%)	246 240
SLOW COOKOFF			
	λ and C fixed	λ and C variable	Experiment
Time to Event (s) Surface Temp. °C	1400 (15%) 206 (6%)	1645 (0.5%) 216 (1%)	1654 218

Figures 9 and 10 show the radial temperature profile within the SSCB at selected times for both fast and slow cookoff. Under fast cookoff conditions (Figure 9) there is a considerable thermal gradient within the SSCB, the temperature is highest at the edge of the cookoff bomb, and thermal runaway commences very close to the surface of the explosive. For slow cookoff (Figure 10) there is a more uniform temperature distribution within the SSCB and the reaction commences closer to the centre of the bomb. Figure 10 also indicates that an appreciable fraction of the RDX is present in the liquid state for approximately two minutes prior to the start of reaction. Recent work using a more extensive thermocouple array within the SSCB has confirmed that melting of the RDX does occur at the centre of the SSCB approximately 100 seconds prior to reaction, although the extent of the melting is less than that shown in Figure 10 [25].

4.2 Multi-term Kinetic Scheme

The chemical decomposition model for RDX described by McGuire and Tarver [3] consists of three reactions, represented by the following sequence:

$$A \xrightarrow{1} B \xrightarrow{2} 2C \xrightarrow{3} D \qquad (21)$$

where A represents RDX, B represents H_2C=N-NO_2, C represents (CH_2+N_2) or (HCN+HNO_2), and D represents the final products. As the decomposition proceeds the concentration of each of the species is described by the following set of coupled rate equations:

$$\frac{dA}{dt} = -k_1 A \tag{22}$$

$$\frac{dB}{dt} = k_1 A - k_2 B \tag{23}$$

$$\frac{dC}{dt} = k_2 B - k_3 C^2 \tag{24}$$

$$\frac{dD}{dt} = k_3 C^2 \tag{25}$$

where the rate constants k_i are defined by $k_i=Z_i\exp(-E_i/RT)$. The source term in the heat flow equation for this model has the form

$$N_A q_1 Z_1 e^{-E_1/RT} + N_B q_2 Z_2 e^{-E_2/RT} + N_C^2 q_3 Z_3 e^{-E_3/RT} \tag{26}$$

where N_A,N_B,N_C and N_D are the respective mole fractions defined such that $N_A+N_B+N_C+N_D=1$.

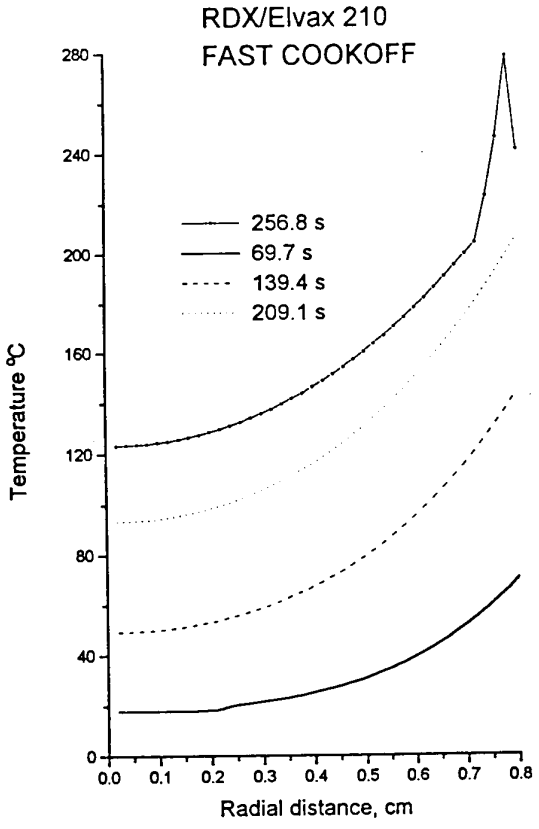

Figure 9: Simulated radial temperature profile within the SSCB at selected times.

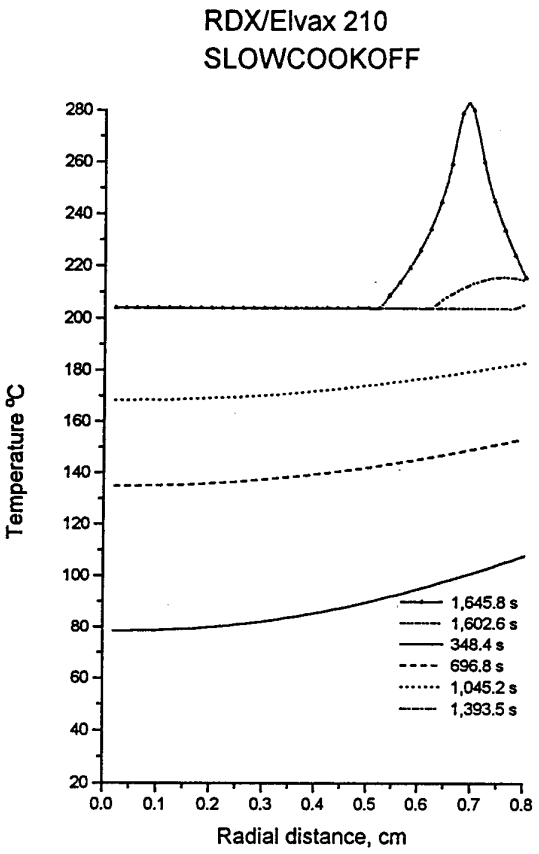

Figure 10: Simulated radial temperature profiles within the SSCB at selected times.

The above kinetic scheme was included in the computer code described in section 4.1, which was then used to model both fast and slow cookoff for RDX/Elvax 210 in the SSCB. The results are shown in Table 4. These indicate that the more sophisticated decomposition scheme provides worse agreement with experiment than does the simple first order scheme. The reason for this is believed to be related to the differing amounts of confinement in the SSCB and ODTX tests. The papers by Tarver et al. [18] and Catalano et al. [17] have shown that the time to explosion is strongly influenced by the void volume of the containment vessel. Even the addition of a relatively small void space in the ODTX experiments resulted in almost a doubling of the time to explosion for LX-04 (85% HMX, 15% binder). In the earlier experimental work of Rogers [10], Zinn and Mader [11], and Zinn and Rogers [16], the explosive samples were less well confined and the explosive decomposition products were easily vented, whereas in the ODTX experiments great care was taken to ensure that none of the gaseous products were allowed to escape from contact with the high explosive sample. Calculations of critical temperatures for the explosives TNT, TATB and LX-10

using a multi-term decomposition scheme similar to the one above gave good agreement with results from ODTX tests, but were appreciably lower than values calculated using the earlier single step schemes [18]. Similar reductions in surface temperature at reaction are observed here for the RDX/Elvax 210 composition shown in Table 4. The SSCB contains a relatively large void space at the top of the cylinder, and the top confining plate contains a small hole which allows access for the thermocouple, and remains unsealed during the test. Hence the gaseous decomposition products are relatively easily vented, and the SSCB is more aptly described by the single step reaction schemes constructed to model the earlier experiments. When the multi-term kinetic scheme is used, as in the results shown in Table 4, the effect is to reduce both the time to explosion and the surface temperature at explosion, for both fast and slow cookoff. A modified form of SSCB test is to be constructed shortly at MRL. This will include pressure transducer diagnostics, and the cylinder will be sealed to ensure that gaseous decomposition products will be contained until the cylinder is ruptured [21]. Under these conditions the SSCB results are expected to agree more closely with the calculated values shown in Table 4.

Table 4: Simulated results for RDX/Elvax 210 (95:5) using Improved Model

FAST COOKOFF			
	First order kinetics	Multi term kinetics	Experiment
Time to Event (s) Surface Temp. °C	263 (7%) 245 (2%)	235 (4%) 226 (6%)	246 240
SLOW COOKOFF			
	First order kinetics	Multi term kinetics	Experiment
Time to Event (s) Surface Temp. °C	1580 (5%) 214 (2%)	1315 (20%) 201 (8%)	1654 218

4.3 Effect of Binder

The calculations to date have used a reference composition consisting of 100% RDX instead of the actual composition, consisting of 95% RDX and 5% Elvax 210. We now consider the effect of this approximation on the accuracy of the calculated results. Data on the thermophysical constants of Elvax 210 are difficult to obtain. A recent paper by Dagley et al. [22] quotes the thermal conductivity of Elvax 265 (a related polymer which should have very similar thermophysical properties to Elvax 210) as 7.14×10^{-4} cal $cm^{-1}s^{-1}$ $°C^{-1}$ at 30°C and 5.24×10^{-4} cal $cm^{-1}s^{-1}$ $°C^{-1}$ at 200°C. These are very close to the thermal conductivity values for RDX used by McGuire et al. [3] of 6.22×10^{-4} cal $cm^{-1}s^{-1}$ $°C^{-1}$ at 20°C and 4.85×10^{-4} cal $cm^{-1}s^{-1}$ $°C^{-1}$ at 160°C. An estimate of the effective thermal conductivity of the RDX/Elvax 210 (95:5) mixture can be made by assuming that the composition consists of spheres of RDX uniformly coated with

Elvax 210. Helsing and Grimvall [23] quote the following expression for the effective thermal conductivity of such a composite system :

$$\lambda_{eff} = \lambda_\alpha + f_\beta \left(\frac{1}{1/(\lambda_\beta - \lambda_\alpha) + f_\alpha/(3\lambda_\alpha)} \right) \qquad (27)$$

where phase β represents the RDX, phase α represents the Elvax 210, and f_α and f_β represent the respective volume fractions. When this expression is used to calculate the thermal conductivity at the lower temperature a value of 6.10×10^{-4} cal $cm^{-1}s^{-1}$ $°C^{-1}$ is obtained; this is very close to the value for RDX at this temperature, indicating that our use of the thermal conductivity of RDX for the effective thermal conductivity of the composite system is quite a good approximation.

The specific heat of Elvax 210 is quoted by Dagley et al. [22] as being 0.57 cal $g^{-1}°C^{-1}$ at 150°C and 0.63 cal $g^{-1}°C^{-1}$ at 220°C, which is considerably higher than the values used by McGuire et al. [3] of 0.24 cal $g^{-1}°C^{-1}$ at 20°C and 0.42 cal $g^{-1}°C^{-1}$ at 350°C for RDX. The effective specific heat of the composite material will still be very close to the RDX value however because the contribution from the Elvax 210 (which is directly proportional to its mass fraction) will be small compared with the contribution from the RDX. Another way to look at this is to consider that the higher specific heat of the Elvax 210 will result in a lower thermal diffusivity for this material. If the thermal diffusivity is calculated using λ from equation (27) then the calculated value is very close to the thermal diffusivity of RDX.

The discussion above is based on the use of partly known and partly inferred thermophysical constants for the binder. Given that these approximate expressions result in estimates for the effective thermal conductivity and specific heat for the composite material which are very close to those for RDX, we feel justified in continuing to omit the binder from the calculations, and to consider the reference composition to consist entirely of RDX. For reasons similar to those discussed above we have also not included in the calculations a term to account for the melting of the binder. For Elvax 210 this occurs around 60°C.

While we expect that neglecting the thermophysical properties of the binder will have little effect on the thermophysical properties of the reference composition, and therefore on the predicted cookoff temperature and time to event, the pressence of the binder is known to have a significant effect on the violence of the reaction event [24].

5. Results of Improved Model for Explosive Mixtures

The results presented in Section 3 have shown that a simple model of the explosive mixtures based on the use of zero order kinetics to describe the reaction decomposition, an Arrhenius temperature dependence for the rate of reaction,

temperature independent thermophysical constants, and allowance for the melting of the RDX, is capable of reproducing the observed experimental trends in the time to reaction and surface temperature at reaction. In Section 4 we showed that by including reactant depletion (ie. first order decomposition reaction) and the temperature dependence of the specific heat and thermal conductivity of the explosive we were able to obtain improved agreement with the experimental results for RDX/Elvax 210 (95:5) at both fast and slow cookoff. We also showed that the decomposition reaction schemes devised by McGuire and Tarver [3], and Drake [2], for ODTX experiments were inappropriate for the SSCB. In this section we improve our models for RDX/PETN/Elvax 210 and RDX/TATB/Elvax 210 by including the relevant refinements described in Section 4.

Our models for the two explosive mixtures are necessarily different. Data on the temperature dependence of the thermal conductivity and specific heat of PETN were unavailable, and so could not be included. PETN however melts at a temperature of approximately 141°C and has a latent heat of fusion of approximately 10 kcal/mole, and so allowance for the melting of both the RDX and PETN was included in the model, together with a first order reaction scheme for both the RDX and PETN. The temperature dependence of the thermal conductivity and specific heat of TATB has been reported by both McGuire and Tarver [3] and Drake [2], and was included in the refined model for RDX/TATB/Elvax 210. First order reaction schemes were employed for both RDX and TATB, although the TATB does not react in the temperature range considered here. No allowance for TATB melting was necessary, since its melting point (320°C [12]) is above the temperature at which reaction occurs in any of our experiments or calculations.

Figure 11 shows the experimental and calculated surface temperature at reaction as a function of PETN content at the slow heating rate. Considerable improvement over the results from the simple model (Figure 1) are observed; there is now good agreement with experiment for an appreciable range of PETN content, although the calculated and experimental results still diverge at 30% to 40% PETN content. This may be due to the neglect of the temperature dependence of the specific heat and thermal conductivity of the PETN, or simply the large scatter in the experimental points. If the high temperature result at 35% PETN content was in error and the true value was closer to the low temperature result then the calculated and experimental curves would be in agreement over the complete range. Figure 12 shows that a similar degree of improvement can be seen in the time to reaction as a function of PETN content at the slow heating rate.

At the fast heating rate the improved model for RDX/PETN/Elvax 210 shows considerably better agreement with experiment than the simple model. Figure 13 shows the surface temperature at reaction as a function of PETN content. The simple model (Figure 5) predicted a rapid decrease in temperature for small amounts of PETN followed by a levelling off at around 30% to 40% PETN content, while experiment showed that the temperature decreased only slowly at small percentages of PETN, and then dropped quickly in the 20% to 40% range. The improved model has corrected these opposing trends; the drop in temperature is now quite small at the lower PETN levels, and the experimental and simulated results agree well to about

20% PETN concentration. For higher levels of PETN content the simulated result is now too high, but this may again be the result of the neglect of the temperature dependence of the thermophysical constants for PETN. Even better agreement can be seen in Figure 14, which shows the time to reaction as a function of PETN content at the fast heating rate. The simple model (Figure 6) showed general agreement, but again the maximum simulated rate of decrease in temperature occured at the wrong end of the range. Figure 14 shows excellent agreement between the simulated curve and a straight line fit to the experimental data.

For RDX/TATB/Elvax 210 there is also generally better agreement with experiment for the improved model. Figure 15 shows surface temperature at reaction as a function of TATB content for the slow heating rate. The simulated results are now closer to the experimental results, although the effect of including the temperature dependence of the specific heat and thermal conductivity has been to reduce the rate of temperature increase with increasing amounts of TATB. The simple model (Figure 3) showed an increase in reasonable agreement with experiment, whereas Figure 15 shows that the improved model predicts that the surface temperature is almost independent of TATB content. Figure 16 shows time to reaction as a function of TATB content at the slow heating rate. The simple model (Figure 4) predicted an increase in time to reaction as the TATB content increased, while experimentally there is a decrease. In Figure 16 the improved model predicts that the time to reaction will be independent of TATB content, and agreement with experiment is considerably better. The very low experimental value at 20% TATB level is also rather suspect, and if this value were higher then there would be excellent agreement with experiment.

At the fast heating rate the improved model has had little effect on the simulated results, although the small changes which have been made appear to have shifted the results slightly away from experiment. Figure 17 shows the surface temperature at reaction as a function of TATB content. The simple model (Figure 7) showed a slight increase in temperature as TATB content increased. Figure 17 however shows that the improved model predicts a very slight decrease with TATB content. A similar discrepancy is shown in Figure 18, which shows time to reaction as a function of TATB content. The simple model (Figure 8) showed a slight increase in time to reaction as the TATB content increased, while experiment shows an even greater increase. Figure 18 however shows that the improved model predicts a very slight decrease in time to reaction as TATB content is increased. One possible explanation for this discrepancy was thought to be the use of equation (9), which may not be valid at the higher levels of TATB concentration. Hence the simulated results shown in Figures 17 and 18 were recalculated assuming that the thermal conductivity of the mixture was given by the mass average of the values for the individual explosives, as used by McGuire and Tarver [3]. This altered the simulated results by less than 0.5% however. We currently have no explanation for the failure of the improved model to predict better agreement with experiment for TATB at the fast heating rate.

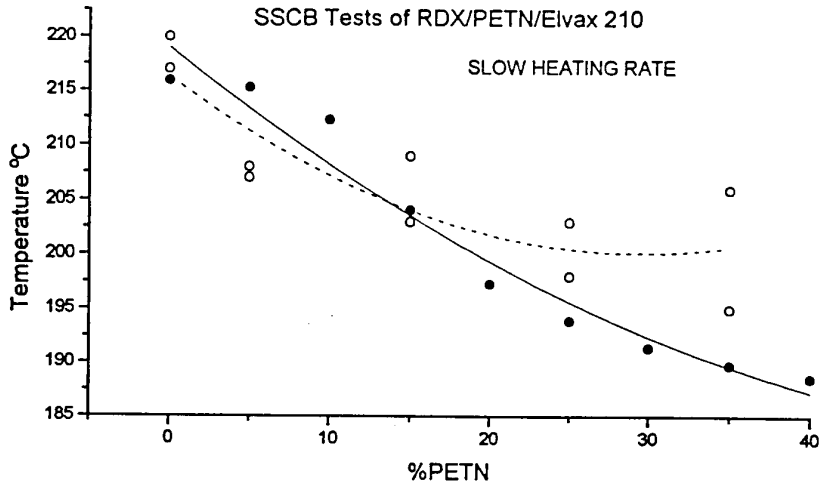

Figure 11: Surface temperature at reaction as a function of PETN content. The open circles are the experimental points and the filled circles are the predictions of the improved model.

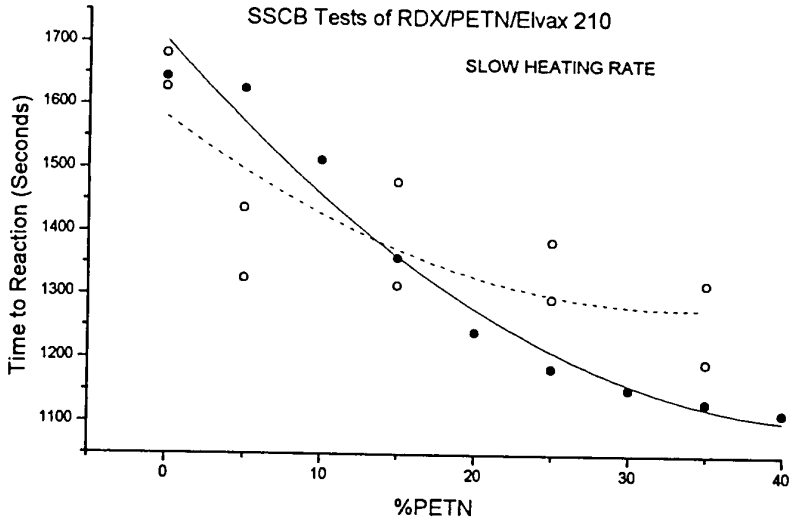

Figure 12: Time to ignition as a function of PETN content. The open circles are the experimental points and the filled circles are the predictions of the improved model.

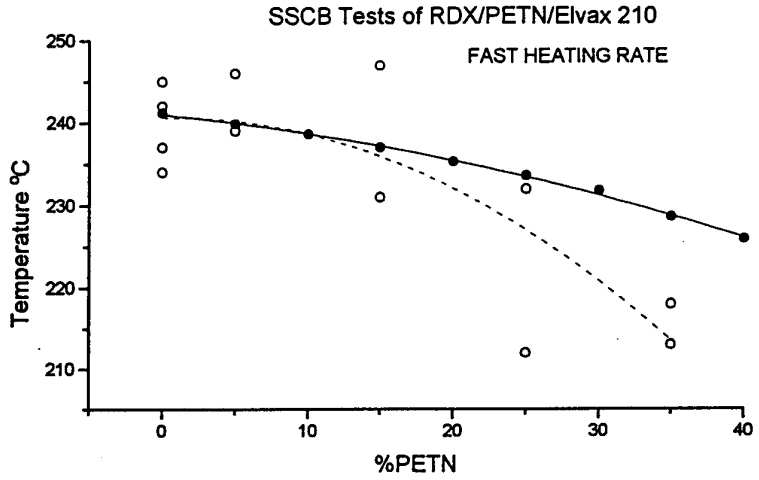

Figure 13: Surface temperature at reaction as a function of PETN content. The open circles are experimental points and the filled circles are the predictions of the improved model.

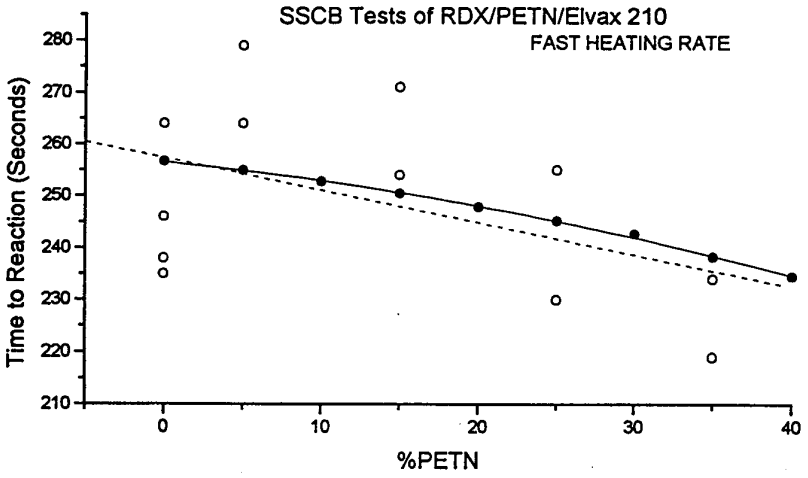

Figure 14: Time to reaction as a function of PETN content. The open circles are the experimental points and the filled circles are the predictions of the improved model.

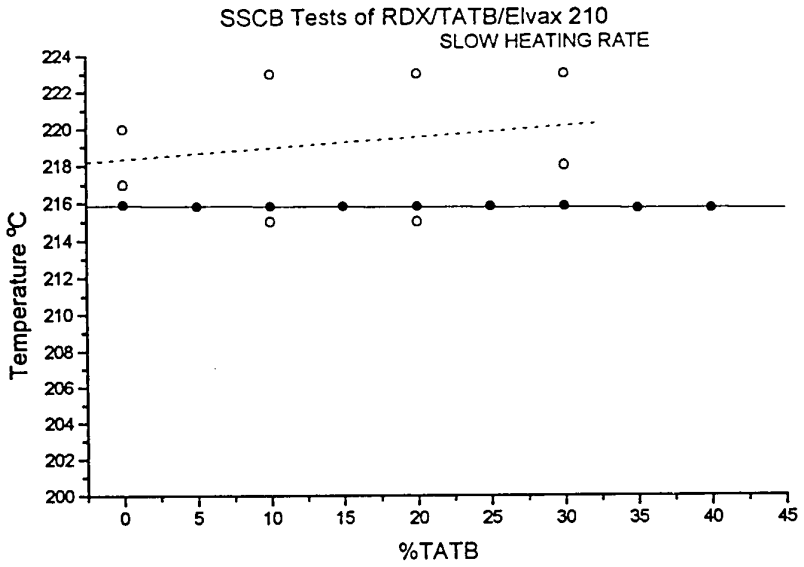

Figure 15: Surface temperature at reaction as a function of TATB content. The open circles are the experimental points and the filled circles are the predictions of the simple model.

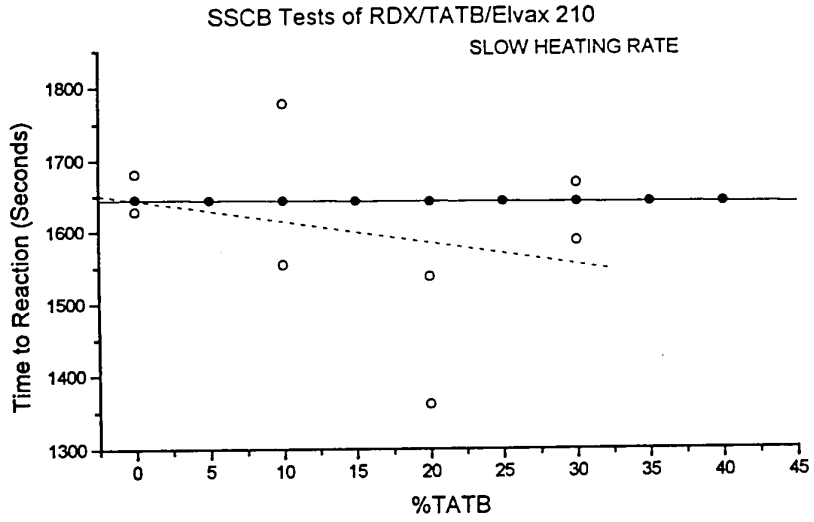

Figure 16: Time to reaction as a function of TATB content. The open circles are the experimental points and the filled circles are the predictions of the improved model.

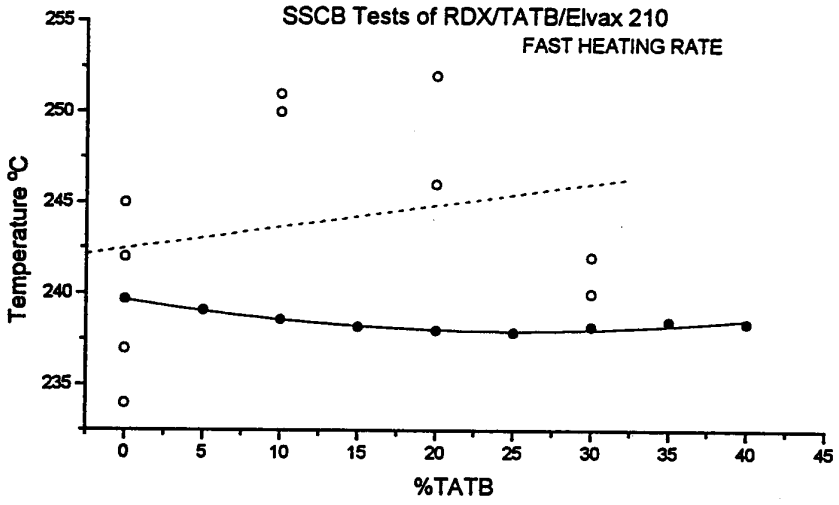

Figure 17: Surface temperature at reaction as a function of TATB content. The open circles are the experimental points and the filled circles are the predictions of the improved model.

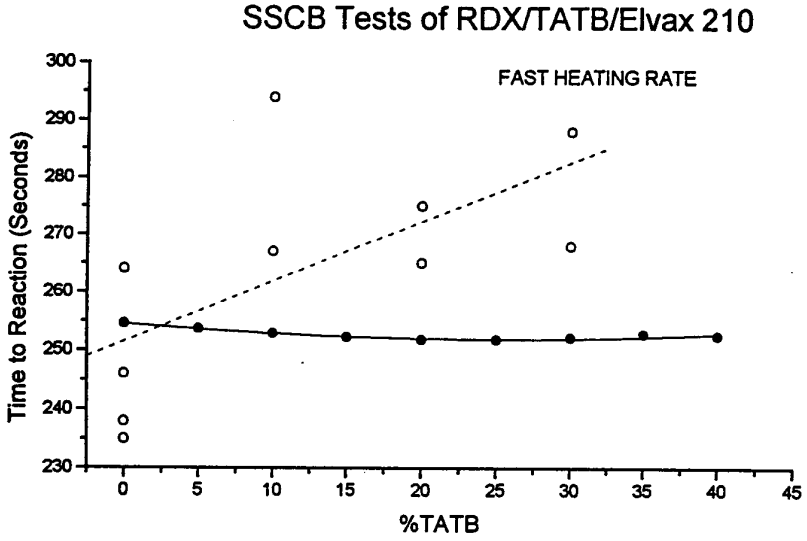

Figure 18: Time to reaction as a function of TATB content. The open circles are experimental points and the filled circles are the predictions of the improved model.

6. Conclusion

We have described the development of a one-dimensional model designed to simulate heat flow in a two-component explosive mixture. The model was implemented in two stages, and at each stage the results of the simulations were compared with experimental values obtained from SSCB tests. In the first stage we neglected the temperature dependence of the thermophysical constants of the explosives, used a zero order kinetic scheme for their thermal decomposition, and only considered melting of the RDX component. Even with these limitations, the simulated results were found to reproduce the overall trends shown by experiment, the only exception being the time to reaction for RDX/TATB/Elvax 210 at the slow heating rate, where the experimental results decreased slightly as the TATB content increased, while the simulated results predicted an increase in time to reaction as TATB content increased.

In the second stage we added various refinements to the model. We included the temperature dependence of the thermal conductivity and specific heat of RDX and TATB, and a term to model melting of the PETN. We also used a first order kinetic scheme for the decomposition of each of the explosives. In general, we found that these refinements greatly improved agreement with the experimental results. For RDX/TATB/Elavax 210 at the fast heating rate however the improved model resulted in a very slight change in the simulated results away from experiment.

Our improved model also considered the effect of a multi-term kinetic scheme to describe the decomposition of the RDX, and this was found to provide poor agreement with the current SSCB results. As discussed in section 4, this is believed to be related to the differing amounts of confinement in the SSCB and ODTX tests.

In conclusion, our calculations clearly illustrate the need to include the temperature dependence of the thermal properties of the material, and a kinetic decomposition scheme appropriate to the degree of confinement, before good agreement between simulated and experimental results can be obtained.

7. Acknowledgements

We thank Dr. I. Dagley for his interest in this work, and for many useful discussions. We also thank Dr. C. Tarver of LLNL for providing a detailed description of the multi-term decompostion scheme for RDX.

8. References

1. Dagley, I.J., Parker, R.P., Montelli, L. and Louey, C.N. (1992). "Mixed High Explosives for Insensitive Booster Compositions". (MRL Technical Report MRL-TR-92-22). Maribyrnong,Vic: Materials Research Laboratory, July 1993.

2. Drake, R.C. (1990) "ODTX Experimental and Thermal Modelling - Summary of Results", AWE Aldermaston, Report ETB No. 221.

3. McGuire, R.R. and Tarver, C.M. (1981) "Chemical Decomposition Models for the Thermal Explosion of Confined HMX, TATB, RDX, and TATB Explosives". Seventh Symposium (International) on Detonation, U.S. Naval Academy Annapolis, Maryland, June 16-19, 1981. NSWC MP 82-334, Naval Surface Weapons Center, 56-64.

4. Victor, A.C. (1992). "Simple Analytical Relationships for Munitions Hazard Assessment". DDESB Explosives Safety Seminar, 18-20 August 1992, Anaheim, California.

5. Private communication, M. Cook, DRA Fort Halstead, August 9, 1993, and P. Haskins, DRA Fort Halstead, September 24, 1993 (during visit to MRL).

6. Parker, R.P. (1989). "Establishment of a Super Small-scale Cookoff Bomb (SSCB) Test Facility at MRL". (MRL Technical Report MRL-TR-89-9). Maribyrnong, Vic: Materials Research Laboratory.

7. Jones, D.A. and Parker, R.P. (1991). "Heat Flow Calculations for the Small Scale Cookoff Bomb Test". (MRL Technical Report MRL-TR-91-12). Maribyrnong, Vic: Materials Research Laboratory.

8. Bowes, P.C. (1984) "Self-heating:evaluating and controlling the hazards", Elsevier Press, 1984.

9. Smith, G.D. (1978) "Numerical Solution of Partial Differential Equations:Finite Difference Methods" Second Edition, Oxford University Press, 1978.

10. Rogers, R.N. (1975). "Thermochemistry of Explosives", Thermochimica Acta **11**, 131.

11. Zinn, J. and Mader, C.L. (1959) "Thermal Initiation of Explosives". J. Applied Physics, **31**, 323-328.

12. Dobratz, B.M. and Crawford, P.C. (1985) "LLNL Explosives Handbook, Properties of Chemical Explosives and Explosive Simulants", UCRL 52997 Change 2, 31 Jan 1985, LLNL, Livermore, CA.

13. Hutchinson, C.D. (1985), "Experimental Studies Concerning the Response of Intermediate Explosives to Thermal Stimuli", Eighth Symposium (International) on Detonation, 1105-1118.

14. Maxwell, J.C. (1873). "Electricity and Magnetism". (1st ed.) Clarendon Press

15. Jeffrey, D.J. (1973). "Conduction through a random suspension of spheres". Proc. R. Soc. Lond. A., 335, 355-367.

16. Zinn, J. and Rogers, R.N. (1962) "Thermal Initiation of Explosives", J. Phys. Chem., 66, 2646-2653.

17. Catalano, E., McGuire, R., Lee, E., Wrenn, E., Ornellas, D. and Walton, J. (1976). "The Thermal Decomposition and Reaction of Confined Explosives", Sixth Symposium (International) on Detonation, San Diego, California, August 24-27, 1976. Office of Naval Research, ACR-221, 214-222.

18. Tarver, C.M., McGuire, R.R., Lee, E.L., Wrenn, E.W. and Brein, K.R. (1978). "The Thermal Decomposition of Explosives with Full Containment in One-Dimensional Geometries", Seventeenth Symposium (International) on Combustion, The Combustion Institute, Pittsburgh, PA, 1407-1413.

19. Ozisik, M.N. (1968) "Boundary Value Problems of Heat Conduction", Dover Publications, Inc., New York, 1978.

20. Farnia, K. and Beck, J.V. (1977) "Numerical Solution of Transient Heat Conduction Equations for Heat-Treatable Alloys Whose Thermal Properties Change with Time and Temperature", Journal of Heat Transfer, **99**, 471-478.

21. Ho, S.Y., Ferschl, T. and Foureur, J. (1993) "Correlation of Cookoff Behaviour of Rocket Propellants with Thermomechanical and Thermochemical Properties" (MRL Technical Report MRL-TR-93-15). Maribyrnong,Vic: Materials Research Laboratory, November 1993.

22. Dagley, I.J., Ho, S.Y., Montelli, L. and Louey, C.N. (1992) "High Strain Rate Impact Ignition of RDX with Ethylene-Vinyl Acetate (EVA) Copolymers". Combustion and Flame, **89**, 271-285.

23. Helsing, J. and Grimvall, G. (1991) "Thermal conductivity of cast irons: Models and analysis of experiments", J. Appl. Phys., **70**, 1198-1206.

24. Dagley,I.J., Spencer, H.J., Louey, C.N. and Parker, R.P. (1989). "An Evaluation of Ethylene-Vinyl Acetate Copolymers as Desensitizers for RDX in Insensitive Booster Compositions Prepared by the Slurry Coating Technique" (MRL Technical Report MRL-TR-89-33). Maribyrnong, Vic: Materials Research Laboratory.

25. Dagley, I.J., Parker, R.P., Jones, D.A. and Montelli, L. (9194). "Simulation and Moderation of the Thermal Response of Confined Pressed Explosive Compositions", in preparation for submission to Combustion and Flame.

SECURITY CLASSIFICATION OF THIS PAGE **UNCLASSIFIED**

REPORT NO.	AR NO.	REPORT SECURITY CLASSIFICATION
DSTO-TR-0090	AR-008-959	Unclassified

TITLE

Simulation of cookoff results in a small scale test

AUTHOR(S)
D.A. Jones and R.P. Parker

CORPORATE AUTHOR
DSTO Aeronautical and Maritime Research Laboratory
GPO Box 4331
Melbourne Victoria 3001

REPORT DATE	TASK NO.	SPONSOR
October 1994	DST 91/185	DSTO

FILE NO.	REFERENCES	PAGES
510/207/0137	25	37

CLASSIFICATION/LIMITATION REVIEW DATE

CLASSIFICATION/RELEASE AUTHORITY
Chief, Explosives Ordnance Division

SECONDARY DISTRIBUTION

Approved for public release

ANNOUNCEMENT

Announcement of this report is unlimited

KEYWORDS

RDX	Energetic materials	Impact shock
Explosives	Decomposition	Sensitivity
Insensitive munitions	Cookoff	

ABSTRACT

The fast and slow cookoff behaviour of two series of candidate insensitive booster compositions based on RDX/Elvax 210, and incorporating various amounts of PETN and TATB, has been numerically simulated using a one-dimensional finite difference code. The model solves a cylindrically symmetric heat flow equation for a mixture of two energetic materials with a time dependent boundary temperature. The temperature dependence of the thermal conductivity and specific heat of each of the explosives is included, as well as the effect of melting, and the effect of different kinetic schemes for the decomposition of the RDX. The simulations accurately reproduce the time to explosion and surface temperature at explosion for varying PETN concentration at both fast and slow heating rates, and also provide good agreement with experiment for varying TATB levels at the slow heating rate. However at the fast heating rate there is a divergence between the simulated results and experiment. The calculations clearly illustrate the need to include the temperature dependence of the thermal properties of the material, and a kinetic decomposition scheme appropriate to the degree of confinement, before good agreement between simulated and experimental results can be obtained.

Simulation of Cookoff Results in a Small Scale Test

D.A. Jones and R.P. Parker

(DSTO-TR-0090)

DISTRIBUTION LIST

Director, AMRL
Chief, Explosives Ordnance Division
Dr B.W. Thorpe
Dr D.A. Jones
Mr R.P. Parker
Library, AMRL Maribyrnong
Library, AMRL Fishermens Bend

Chief Defence Scientist (for CDS, FASSP, ASSCM)	1 copy only
Director, ESRL	
Head, Information Centre, Defence Intelligence Organisation	
OIC Technical Reports Centre, Defence Central Library	
Officer in Charge, Document Exchange Centre	8 copies
Senior Defence Scientific Adviser	
Air Force Scientific Adviser, Russell Offices	
Scientific Adviser - Policy and Command	
Senior Librarian, Main Library DSTOS	
Librarian, DSD, Kingston ACT	
Serials Section (M List), Deakin University Library, Deakin University, Geelong 3217	
NAPOC QWG Engineer NBCD c/- DENGRS-A, HQ Engineer Centre, Liverpool Military Area, NSW 2174	
ABCA, Russell Offices, Canberra ACT 2600	4 copies
Librarian, Australian Defence Force Academy	
Head of Staff, British Defence Research and Supply Staff (Australia)	
NASA Senior Scientific Representative in Australia	
INSPEC: Acquisitions Section Institution of Electrical Engineers	
Head Librarian, Australian Nuclear Science and Technology Organisation	
Senior Librarian, Hargrave Library, Monash University	
Library - Exchange Desk, National Institute of Standards and Technology, US	
Acquisition Unit (DSC-EO/GO), British Library, Boston Spa, Wetherby, Yorkshire LS23 7BQ, England	
Library, Chemical Abstracts Reference Service	
Engineering Societies Library, US	
Documents Librarian, The Center for Research Libraries, US	
Army Scientific Adviser, Russell Offices - data sheet only	
Navy Scientific Adviser - data sheet only	
Director General Force Development (Land) - data sheet only	
DASD, APW2-1-OA2, Anzac Park West, Canberra ACT - data sheet only	
SO (Science), HQ 1 Division, Milpo, Enoggera, Qld 4057 - data sheet only	
Librarian - AMRL Sydney - data sheet only	
Counsellor, Defence Science, Embassy of Australia - data sheet only	
Counsellor, Defence Science, Australian High Commission - data sheet only	
Scientific Adviser to DSTC Malaysia, c/- Defence Adviser - data sheet only	
Scientific Adviser to MRDC Thailand, c/- Defence Attache - data sheet only	